

Nanolime for the consolidation of lime mortars: a comparison of three available products

OTERO, Jorge, STARINIERI, Vincenzo <<http://orcid.org/0000-0002-7556-0702>> and CHAROLA, A. Elena

Available from Sheffield Hallam University Research Archive (SHURA) at:
<http://shura.shu.ac.uk/21609/>

This document is the author deposited version. You are advised to consult the publisher's version if you wish to cite from it.

Published version

OTERO, Jorge, STARINIERI, Vincenzo and CHAROLA, A. Elena (2018). Nanolime for the consolidation of lime mortars: a comparison of three available products. *Construction and Building Materials*, 181, 394-407.

Copyright and re-use policy

See <http://shura.shu.ac.uk/information.html>

Nanolime for the consolidation of lime mortars: a comparison of three available products

J. Otero^{a*}, V. Starinieri^a, A. E. Charola^b

^a *Materials and Engineering Research Institute, Sheffield Hallam University, Sheffield, S1 1WB, UK*

^b *Museum Conservation Institute, Smithsonian Institution, Washington DC, USA*

* corresponding author: Tel: +44 1142253500; Fax: +44 114 225 3501; b5039083@my.shu.ac.uk.

KEYWORDS: Nanolime; Nanoparticles; Calcium hydroxide; Consolidation; limestone; Lime mortar; Calosil; Nanorestore

Abstract. Nanolime products are one of the most promising consolidation methods for historic calcareous substrates. Whilst the popularity of nanolime has been growing, its consolidation mechanism still needs to be fully understood when applied to highly porous substrates. The aim of this paper is to compare the three available nanolime products in terms of consolidation efficacy on lime mortar specimens. It is shown that repeated applications of a low concentrated nanolime can increase the superficial cohesion and the mechanical strength of the mortar within 1cm from the surface, while also reducing porosity, number of micro-pores and capillary water absorption coefficient. Nanorestore Plus® yielded the highest short-term consolidation effect. However, L'Aquila nanolime showed a higher durability which was attributed to a better developed crystalline structure.

1. Introduction

The consolidation of degraded calcareous materials is one of the main challenges in the conservation of historic structures. Calcareous substrates degrade by weathering processes such as crystallisation of salts, biological activity, freeze-thaw action and chemical attack by acid atmospheric pollutants [1-3]. Consolidants can help in recovering the strength of degraded materials as well as decreasing the deterioration rate of the substrate. In general, suitable consolidants must meet the following criteria: i) be physically, mechanically and chemically compatible with the substrate; ii) have a good adhesion to the substrate; iii) increase the substrate's mechanical properties; iv) not induce colour or aesthetic changes to the substrate; v) reduce porosity but not hamper moisture transport through the substrate. The effectiveness of the consolidation depends on the interaction of a number of factors such as the

29 characteristics of the substrate, the properties of the consolidant and its compatibility with the substrate, and the
30 application methods and conditions [4].

31

32 Limewater, which is a saturated solution of calcium hydroxide with a maximum of concentration of 1.5g/L with
33 lime particles in a colloidal suspension [5], has been used over centuries to consolidate deteriorated limestone or
34 plaster. It has the advantage of being durable and compatible with the substrate as it is based on the precipitation of
35 calcium carbonate into the pores of the treated material by reaction of the calcium hydroxide with the atmospheric
36 carbon dioxide (CO₂). The main constraint of the limewater technique is a low consolidation depth due to limited
37 penetration of carbon dioxide into the substrate [6]. Furthermore, the application of limewater can cause whitening
38 of the treated surface. The effectiveness of limewater has been greatly discussed in literature. According to Price et
39 al. [7] when using limewater most particles are deposited within 2 mm from the surface yielding an ineffective
40 consolidation. Price's research has led some stone conservators to be skeptical of this treatment. Nonetheless,
41 Brajer [8] demonstrated that a prolonged uninterrupted application produces a noticeable consolidation effect and
42 some authors brought up new perspectives to its practical work such as the use of lime poultices and of an
43 increased number of limewater applications [3, 9, 10].

44

45 During the last century, organic consolidants (i.e. synthetic polymers, such as Paraloid B-72, Mowilith 30 and
46 Primal AC33) were extensively used in restoration treatments for calcareous materials due to their immediate
47 strength enhancement, ease of application and the limitations shown by limewater [11]. These consolidants proved
48 to be effective in the short and medium term for some calcareous substrates. However, the low compatibility with
49 the mineral substrate and their short durability caused more substrate degradation in the long term, particularly in
50 environments where temperatures increase above 40°C [3, 9, 11]. Specifically, physical and mechanical
51 incompatibility between organic consolidants and calcareous substrates can cause crack development, aesthetic
52 changes and interference with future treatments [12, 13], sometimes with severe consequences [14, 15].

53

54 Nanolimes were developed to overcome the limitations of the traditional limewater treatment. Their consolidating
55 effect takes place by the same mechanism as for the limewater technique but the smaller size of the lime particles
56 (nanoscale) improves their performance. The advantages of nanolime compared to limewater are: i) nanolimes
57 contain higher amounts of calcium hydroxide particles; ii) lime nanoparticles are more reactive due to their higher

58 specific surface thus increasing the carbonation rate; iii) nanolimes penetrate deeper into the substrate because of
59 their smaller particle size; iv) nanolimes have better colloidal stability due to their smaller particle size and the
60 electrostatic repulsion forces between them; and, v) reduced whitening of the treated surface when nanolimes are
61 used. An overview of nanolime synthesisation methods and use as a consolidant for calcareous substrates can be
62 found elsewhere [16].

63

64 The first nanolime to become available on the market was Calosil® (IBZ-Salzchemie GmbH & Co.KR, Germany)
65 in 2006, followed by Nanorestore® (CSGI - University of Florence, Italy) in 2008. Recently, the University of
66 L'Aquila has patented a new method to synthesise nanolime where nanoparticles are produced by an anion
67 exchange process at ambient room conditions in aqueous suspensions [17-19]. Nanolime produced through this
68 method is currently in the process of being commercialised.

69

70 Both Calosil and Nanorestore have been extensively used for the conservation of wall paintings and stuccoes,
71 achieving good re-adhesion of detached particles or pigment flakes [5, 16, 20] and consolidating powdering
72 surfaces [15, 20]. However, the effectiveness of the nanolimes decreases when mass consolidation of a porous
73 substrate such as deteriorated stone or mortar is required [21-23]. The effectiveness of nanolime as a consolidant
74 appears to be influenced by several factors: i) multiple applications of low nanolime concentration suspensions (i.e.
75 5 g/L) reduce the accumulation of consolidating product near the surface and improves the yield of carbonation
76 within the pores [24, 25]; ii) the type of alcohol used can influence the nanolime deposition in the pores [26, 27] as
77 well as the carbonation process [28], iii) external factors such as relative humidity (RH) and exposure time appear
78 to influence the carbonation rate and precipitation of polymorphs [29, 30]; iv) age and storing temperature of the
79 nanolime affects the conversion of $\text{Ca}(\text{OH})_2$ particles into Ca-alkoxides which can decrease its effectiveness [31].

80

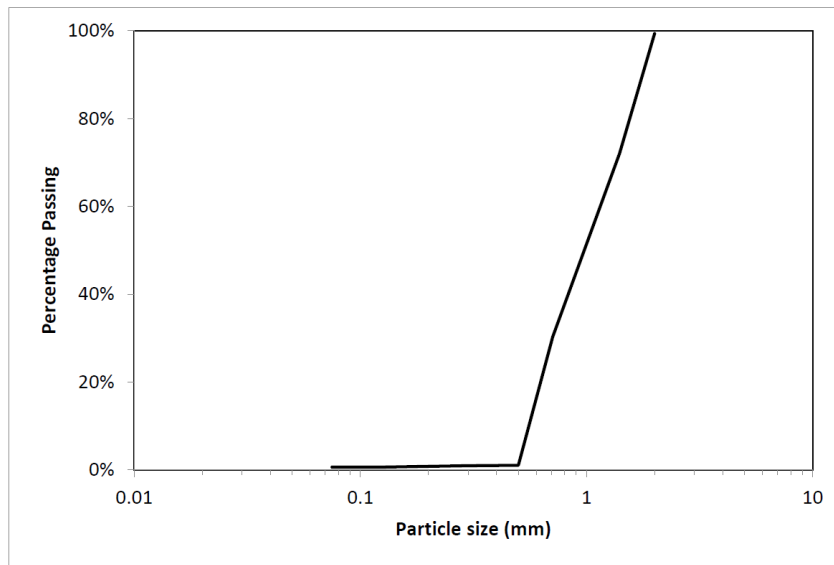
81 The aim of this work is to compare the consolidation effectiveness of the three available nanolime products on lime
82 mortars and investigate their long term performance. The influence of the nanolime treatments on mortar
83 superficial cohesion, water absorption by capillarity, drying rate, drilling resistance, pore structure and aesthetic
84 properties have been investigated.

85

86 **2. Materials and methods**

87 *2.1 Lime and sand*

88 Singleton Birch Ultralime CL90 ($\geq 98\%$ Ca(OH)_2 , measured by XRD and XRF) and silica sand from Pentney
89 (UK) were used throughout this work for the mortar mixes. The sand grading is shown in Figure 1. The
90 mineralogical composition of the sand, which was determined by XRD (*PANalytical XPert PRO*) using Rietveld
91 refinements, is 96.3% Quartz (SiO_2 , ICSD #00-046-1045) and 3.7% Potassium Feldspar (KAlSi_3O_8 , ICSD #01-076-
92 0831).



93
94 **Figure 1.** Sand grading curve

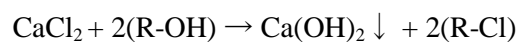
95
96 *2.2 Nanolime*

97 Three nanolime dispersions were used throughout this work:

- 98 - **Nanorestore Plus Propanol 5®** (CSGI Consortium - University of Florence, Italy): 5 g/L calcium
99 hydroxide in 2-propanol. Particle size 100-300 nm. This dispersion is referred to as NAN.
- 100
- 101 - **Calosil IP5®** (by IBZ Salzchemie GmbH & Co.KG, Germany): 5 g/L calcium hydroxide in 2-propanol.
102 Particle size 50-150 nm. This dispersion is referred to as CAL.
- 103

- 104 – **Nanolime synthesised through the method developed by Taglieri et al [17] at the University of**
105 **L'Aquila:** 5 g/L calcium hydroxide in 50-50% water - 2-propanol. Particle size 20-80 nm. This dispersion
106 is referred to as LAQ.

107
108 LAQ was synthesized through an anionic exchange process carried out at room temperature and ambient pressure
109 by mixing under moderate stirring an anion exchange resin (Dowex Monosphere 550A OH from Dow Chemical)
110 with an aqueous calcium chloride solution following a methodology described by Taglieri et. al. [17, 18] and Volpe
111 et. al. [19]. When these two components are mixed together, the substitution of OH groups in the resin with
112 chloride ions (Cl⁻) in solution leads, in conditions of supersaturation, to the formation of pure Ca(OH)₂
113 nanoparticles, following the reaction:



114
115
116
117 The concentration of chloride was monitored during the process (Vernier Chloride Ion-Selective Electrode CL-
118 BTA) and when this reached a constant value below 30 mg/L, the stirring was stopped and the aqueous suspension
119 was separated from the resin by means of a sieve (80µm). The supernatant water was then extracted through a
120 pipette and replaced with 2-propanol in order to maintain a concentration of 5 g/L in a 50-50% vol. water-2-
121 propanol solvent. This is considered the optimal formulation for this nanolime in terms of carbonation and kinetic
122 stability [18, 32].

123
124 The decrease rate of chloride content during the synthesis was very rapid, with about 97% of the reduction
125 occurring within the first minute of the process. The synthesis was stopped after 15 minutes when the ion exchange
126 process was completed (zero kinetic exchange), with a total reduction of chloride content of 99.82% and a residual
127 chloride content of 0.18% (29.4 mg/L). Similar results have been reported by Taglieri et. al. [17-19, 32].

128 129 *2.3 Mortar preparation and testing*

130 Mortars were produced with a volumetric binder:sand ratio of 1:2.5 to a constant flow of 16 cm measured
131 according to BS EN 1015-3:1999 [33]. Although mix proportions are expressed by volume, mortars were batched

132 by weight after accounting for component densities, which were measured in accordance with BS EN 459-2:2010
133 [34]. The water:binder ratio was 1.56 to obtain the desired flow. Mortars were produced by mixing the dry
134 ingredients with water in a Hobart mixer. The mix protocol was as follows: 1) dry mix sand and lime for 2 minutes
135 at 62 rpm; 2) add water while continuing mixing at 62 rpm for 30 s; 3) stop the mixer for 30 s and scrape the mixer
136 bowl; 4) mix for 5 min at 125 rpm. Samples were cast in 40×40×160 mm steel moulds in two layers and vibration-
137 compacted. Immediately upon floating off the fresh mortar, the moulds were transferred to a temperature and
138 humidity controlled room maintained at 20 °C and 65% RH. Mortar beams were de-moulded after 5 days and
139 stored in the same room for the following 23 days. On the 28th day of curing, each prism was cut into 4 cubes
140 measuring approximately 40×40×40 mm prior to curing for further 28 days in the same conditions.

141

142 The mineralogical composition of the mortar was determined by X-Ray Diffraction. Samples obtained from the
143 core of the cube were ground and sieved through an 80 µm sieve mesh and placed over an XRD zero-background
144 sample holder; the XRD patterns were recorded with a step size of 0.026°2θ, in the angular range 5-70°2θ.
145 Quantitative analyses were carried out by means of Rietveld refinement [35, 36]. X-ray data were fitted using the
146 pseudo-Voigt profile function. Specimen displacement, polynomial coefficients for the background function, lattice
147 parameters, profile parameters, and Gaussian and Lorentzian profile coefficients were refined. Quantitative analysis
148 by Rietveld refinement shows the mineralogical composition of the mortar is 82.3% Quartz (SiO₂, ICSD #00-046-
149 1045) and 17.7% Calcite (CaCO₃, ICSD #00-005-0586).

150

151 *2.4 Nanolime characterisation*

152 The size, shape and degree of agglomeration of the calcium hydroxide particles in the three nanolime products were
153 determined by TEM (Philips CM200), while the crystalline phase was analysed by XRD. TEM samples were
154 prepared by dispersing 0.2 ml of nanolime suspension in 20 ml of ethanol and placing a few drops of the resulting
155 liquid on a carbon-coated copper grid. XRD samples were prepared by using the zero-background silica sample
156 holder. Both TEM and XRD samples were prepared in nitrogen atmosphere, to prevent carbonation of the lime.

157

158 The kinetic stability (KS) of the three products was determined by turbidity measurements, analysing their
159 absorbance at $\lambda = 600$ nm by means of a UV/VIS Spectrophotometer (UV-VIS Spectrophotometer Varian
160 50SCAN). Before the test, nanolimes were agitated, instead of sonicated. Sonicating has been the normal practice

161 in previous studies [18, 20, 26, 28], however, agitation was preferred in this work to simulate in-situ conditions
162 where conservators normally have no access to an Ultrasonic Bath. Measurements were taken over a period of up
163 to 2 hours. The relative kinetic stability (KS %) was calculated using the following formula:

$$KS \% = 1 - [(A_0 - A_t) / A_0] \times 100$$

166
167 Where A_0 is the starting absorbance and A_t the absorbance at time t , both at a wavelength of 600 nm [5, 28]. KS %
168 decreases as a result of the nanoparticles settling; values range from 0 (unstable dispersion) to 100 (no deposition of
169 nanoparticles).

171 *2.5 Nanolime carbonation process characterisation*

172 The carbonation process was investigated by means of TEM, SEM (SEM, NOVA 200 NanoSEM 450) and XRD.
173 For TEM observations, samples were prepared as described in section 2.4 and exposed to air for 1 minute prior to
174 carrying out the observations. For SEM investigations, 0.10 ml of each suspension were placed on a copper SEM
175 sample holder and exposed to outdoor conditions in a sheltered area ($T \approx 5-15^\circ\text{C}$, $\text{RH} \approx 60-80\%$) for 7 days prior to
176 carrying out the observations. SEM micrographs were taken with an ETD detector, a working distance of
177 approximately 3 mm, an optimum accelerating voltage of 15 kV and a spot size of about 30 nm. Specimens were
178 coated with a 20 nm thick layer of gold using a Quorum Q150T coater unit to prevent surface charging.

179
180 Samples for XRD were prepared by exposing 0.12 ml of each suspension (NAN, CAL and LAQ) to outdoor
181 conditions in the same sheltered area mentioned previously for 1 hour and 7 days prior to analysing by the
182 diffractometer. XRD patterns were recorded in step size of $0.026^\circ 2\theta$. Each experimental diffraction pattern was
183 elaborated by means of a Profile Fit Software (HighScorePlus, PANalytical), and each crystalline phase was
184 identified using the ICSD and ICDD reference databases. Quantitative analyses were carried out by means of
185 Rietveld refinements.

187 *2.6 Nanolime treatment application*

188 Each of the three nanolimes was agitated and applied by brush on the top face (as cast) of three 40x40x40 mm
189 mortar cubes, allowing the nanolime to be fully absorbed by the mortar between two consecutive brushstrokes.
190 Nanolimes were also agitated between each brushstroke. The treatment was continued until no further absorption
191 was observed for a period of at least one minute after a brushstroke. At this time, the application was interrupted
192 and was repeated 24 hours later when the specimen was dry. Samples were weighed before and after each
193 application (after full evaporation of the solvent) to determine the total amount of nanolime absorbed by the mortar.
194 The treatment was considered complete when each mortar cube absorbed 500mg of calcium hydroxide
195 (approximately 100ml of nanolime). This required about 20 consecutive days of application for each nanolime.
196 Upon treatment completion, the samples were stored outdoor in the sheltered area for a period of 28 days ($T \approx 5-$
197 15°C , $\text{RH} \approx 60-80\%$). A set of untreated control samples was also stored in the same conditions.

198

199 *2.7 Evaluation of treatment effectiveness*

200 Following 28-day outdoor exposure, the mortar cubes were dried to constant mass at 60°C in a fan assisted oven
201 and subsequently stored in a desiccator until testing. The effectiveness of the nanolime was evaluated by means of
202 the tests described below.

203

204 The influence of the treatments on pore size distribution and porosity of the mortars was investigated by Mercury
205 Intrusion Porosimetry (MIP) using a PASCAL 140/240 instrument. Each test was carried out on one fragment
206 measuring approximately 5x5x10 mm collected within 5 mm from the top surface (as cast) of both treated and
207 control samples. The samples were dried in a fan-assisted oven at 60°C until constant weight prior to testing. The
208 mercury contact angle was taken to be 140° .

209

210 The water absorption coefficient by capillarity (WAC) of both treated and control samples was measured according
211 to EN 13755 [37]; three samples being tested for each mortar. Upon completion of this test, once asymptotic water
212 absorption was reached, samples were immersed in water for 24 hours and their apparent porosity was calculated
213 following ASTM C 97-96 (American Society for Testing and Materials, 1996) [38], although the actual immersion
214 time was half of that recommended in this standard. Their drying behaviour was sequentially calculated according
215 to CEN EN 16322 [39]. This sequence simulates a real situation in an outdoor condition (cycles of dry-wet-dry).

216

217 The influence of the nanolime treatments on the surface cohesion of the mortar was evaluated by means of the
218 'Scotch Tape Test' (STT) carried out in accordance with ASTM D3359 [40]. The test was performed on both
219 treated and control samples and results taken as the average of 9 measurements per sample.

220

221 The consolidation effectiveness of the three nanolimes was also assessed by means of a Drilling Resistance
222 Measurement System (DRMS) from SINT-Technology. The DRMS measures the force required to drill a hole at
223 constant rotation (rpm) and lateral feed rate (mm/min). It is generally considered the most suitable methodology for
224 quantifying consolidation effectiveness and depth of penetration of consolidants, particularly in soft stones [41, 42].
225 Tests were performed on both treated and control mortar cubes using drill bits of 5 mm diameter, a rotation speed
226 of 200 rpm, a rate of penetration of 15 mm/min and a drilling depth of 20 mm. Drilling resistance values per each
227 treatment were calculated as the mean of 6 tests carried out on 2 cubes per each of the nanolimes.

228

229 The surfaces of both treated and control samples were observed under a Scanning Electron Microscope in order to
230 evaluate the morphology and distribution within the pores of the calcite crystals originated from the carbonation of
231 nanolime.

232

233 Any surface colour variations induced by the nanolime treatments were evaluated with a spectrophotometer
234 (Minolta CM508D Colorimeter) with the CIELab system [43]. 30 measurements were taken in different areas of
235 the surface of each of the treated and control mortar cubes. Total colour variation (ΔE) was calculated by the
236 formula:

$$\Delta E^* = \sqrt{\Delta L^{*2} + \Delta a^{*2} + \Delta b^{*2}}$$

237 where ΔL^* , Δa^* and Δb^* are the change in luminosity for white-black, red-green and blue-yellow parameters,
238 respectively.

239

240 The durability of the treatments was evaluated using a QUV/SE Accelerated Weathering Tester from Q-Lab
241 Europe Ltd. Both treated and control mortar cubes were exposed to alternating cycles of UV light and moisture
242 condensation at controlled temperatures in accordance to ASTM G154 CYCLE 4 [44] for a period of 340 hours.
243 Each UV cycle has duration of 8 hours and uses an irradiance of 1.55 W/m^2 at a temperature of $70 \text{ }^\circ\text{C}$. The moisture

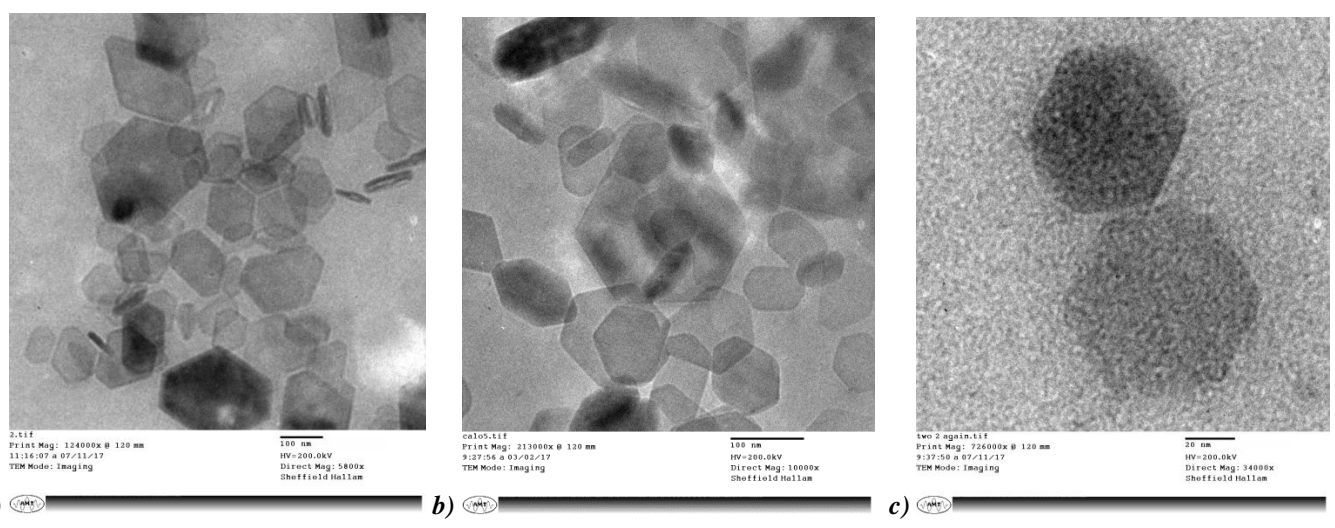
244 condensation cycles are carried out at 50 °C with no UV irradiation. The influence of the accelerated weathering on
245 the mortars surface colour and drilling resistance were assessed by colorimetry and DRMS as described above.

246

247 3. Results and Discussion

248 3.1 Characterisation of the nanolime suspensions

249 Figure 2 shows TEM photomicrographs of the three nanolime products. Hexagonal Ca(OH)_2 nanoparticles with
250 identical morphology can be observed in all three of the nanolimes. The crystals tend to agglomerate due to the
251 nanoparticle phenomenon caused by their high surface energy [26, 28, 31] (Figures 2a and 2b). The size of the
252 observed nanoparticles is 250 - 100 nm for NAN (Figure 2a), 150 - 80 nm for CAL (Figure 2b) and 80 - 20 nm for
253 LAQ (Figure 2c). These results are in line with those reported by the developers of the three products [5, 17-20, 45,
254 46].



255 **a)** **b)** **c)**
256 **Figure 2.** TEM images of: a) NAN; b) CAL; c) LAQ. Please note that the magnification bar is 100 nm for NAN and CAL, and
257 only 20 nm for LAQ.
258

259 The XRD analysis in nitrogen atmosphere (Fig. 3) shows that the only crystalline phase of the three nanolimes is
260 Portlandite (Ca(OH)_2 , ICSD #01-087-0674), confirming the results of the observations by TEM. For the three
261 samples the strongest peak corresponds to the {001} basal plane. However, XRD Rietveld refinements showed that
262 LAQ Ca(OH)_2 particles have a preferred orientation to the side plane {010}. NAN and CAL did not show any
263 significant preferred orientation. The Rietveld refinement factors are included in Table 1.

264

Table 1. Rietveld refinement factors of samples dried in Nitrogen atmosphere and exposed to air in outdoor conditions (60-80%RH) for 1h and 7 days.

	Nitrogen			1 hour in air			7 days in air		
	NAN	CAL	LAQ	NAN	CAL	LAQ	NAN	CAL	LAQ
R-expected	10.1	9.35	13.89	20.24	20.24	20.03	19.53	15.67	20.03
R-profile	11.69	7.98	11.77	16.13	16.13	15.64	18.52	16.31	15.64
Weighed R profile	14.66	10.38	16.11	20.67	20.67	20.17	24.1	20.81	20.17
Goodness of fit	3.49	1.23	4.34	2.04	2.04	3.01	1.52	1.76	4.31
Phase proportions	100% P	100% P	100% P	90.3% C 9.7% P	100% P	100% C	100% C	75.8% C 24.2% V	100% C
Direction of preferred orientations	NPO	NPO	10	NPO	NPO	NPO	NPO	NPO	104

NPO (No preferred orientation), P (Portlandite); C (Calcite); V (Vaterite)

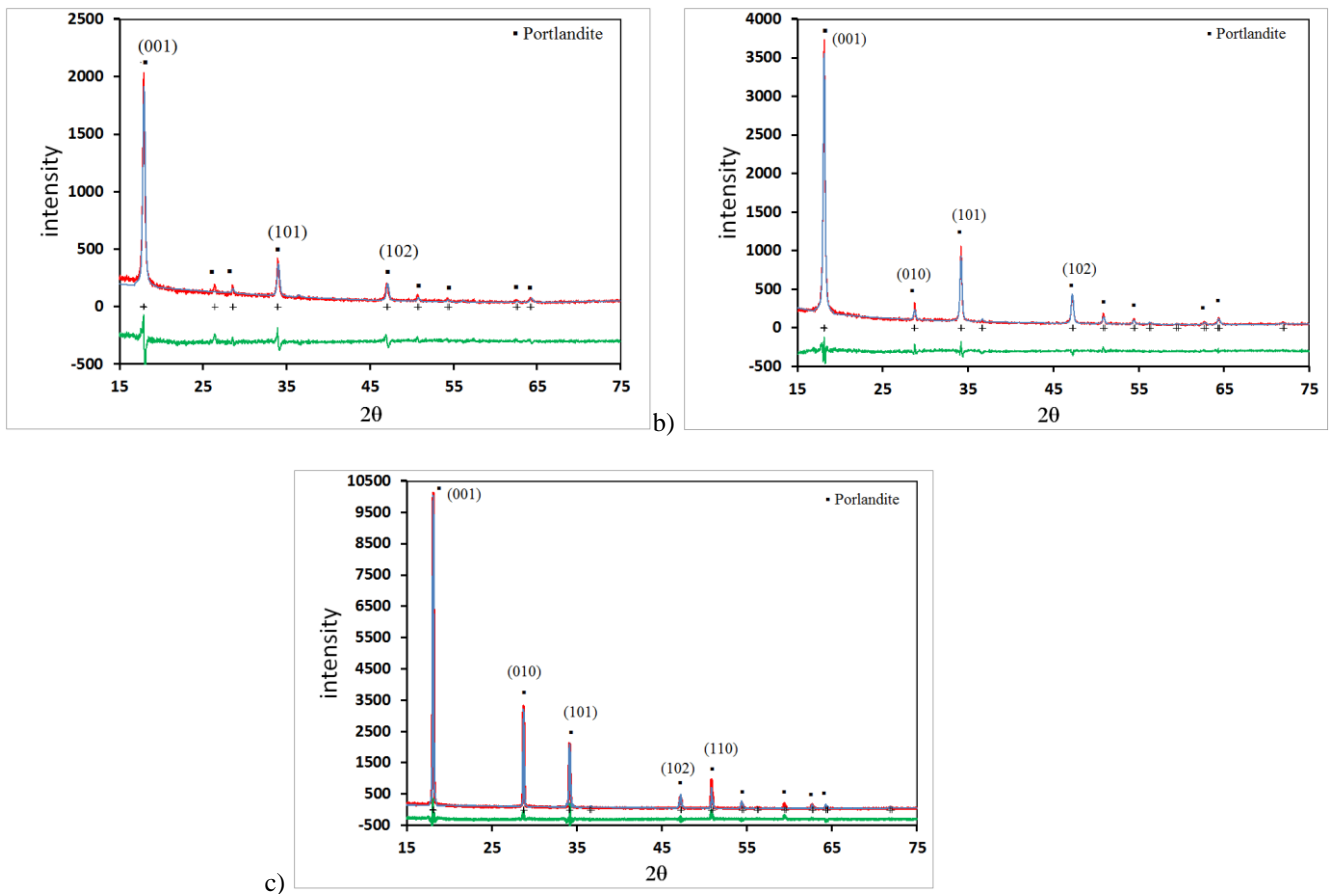
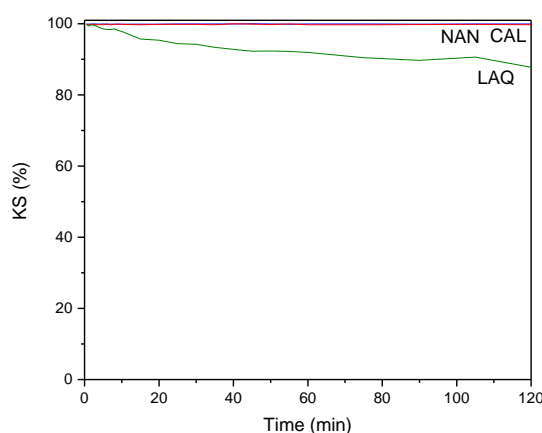


Figure 3. XRD patterns for NAN (a), CAL (b) and LAQ (c) samples dried in nitrogen atmosphere. Red line corresponds to Intensity observed, blue line to Intensity calculated and green line to the Intensity observed - Intensity calculated difference curve. The crystal phases are shown in brackets and the "+" symbol corresponds to the main peaks.

Figure 4 shows the absorbance (at 600nm) of NAN, CAL and LAQ dispersions over a period of 2 hours following a moderate agitation. A high colloidal stability was observed for NAN and CAL $\text{Ca}(\text{OH})_2$ nanoparticles. Previous

274 studies have shown that NAN and CAL nanolimes can keep the colloidal state for more than one week [47]. In
275 contrast, LAQ $\text{Ca}(\text{OH})_2$ nanoparticles start to settle about 2 min after agitation (sedimentation rate $\approx 6\%$ per h) and
276 that 12% of the particles settle after 2 hours of the testing period. This sedimentation process is considerably slower
277 than that occurring in limewater, where more than 90% of the particles settle in 2 hours [48]. The colloidal stability
278 of LAQ dispersion during the first 2 minutes after agitation can be considered acceptable for practical purposes as
279 most of the particles remain in colloidal state for the whole length of each application [28]. High colloidal stability
280 is critical to prevent the formation of undesired surface whitening as colloidal particles penetrate better into the
281 pores reducing accumulation on the surface [48].



282

283 **Figure 4.** Kinetic stability KS (%) of NAN, CAL and LAQ dispersions

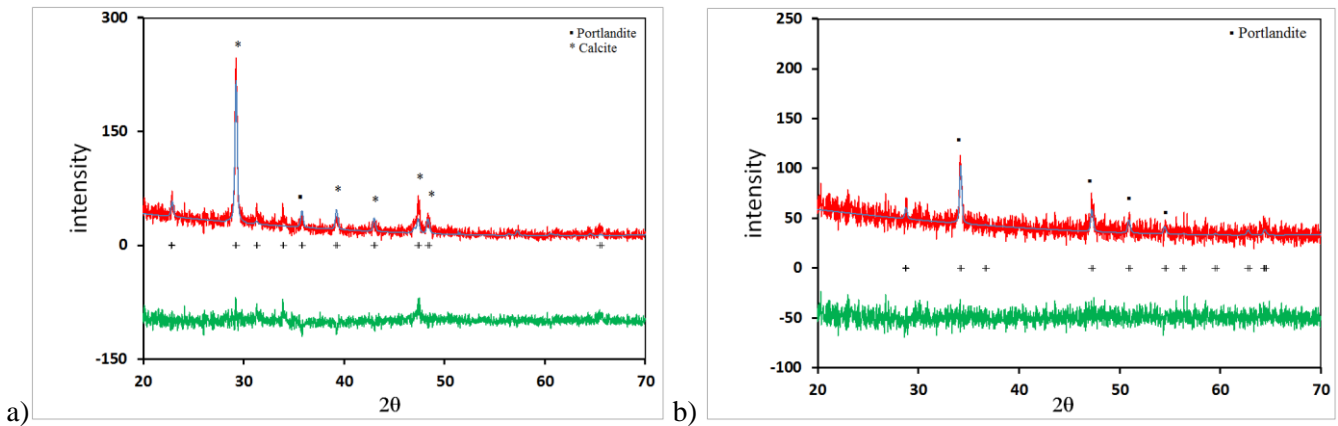
284

285 3.2 Nanolime carbonation process

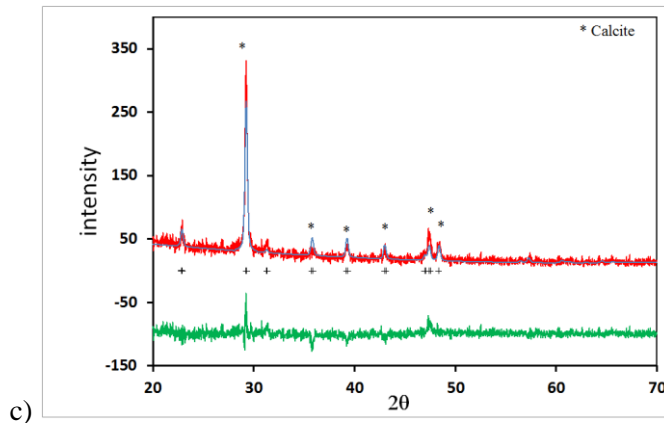
286 The XRD patterns of nanolimes exposed to air for 1 hour (Fig. 5) show the LAQ nanoparticles to be the most
287 reactive, with calcite (ICSD # 01-085-1108) being the only detected crystalline phase (Fig. 5c). NAN nanoparticles
288 (Fig. 5a) also showed good reactivity within the 1 hour of air exposure time, with 90.3% of the sample being
289 composed of calcite (ICSD # 01-072-1652) and 9.7% of portlandite (ICSD # 01-087-0674). The only crystalline
290 phase detected for CAL was portlandite (ICSD # 01-072-0156), indicating a slower carbonation process (Fig. 5b).
291 The relatively high background combined with broad and weak Bragg peaks recorded for these samples suggest the
292 presence of poorly crystalline phase(s) (Fig. 5).

293

294



295



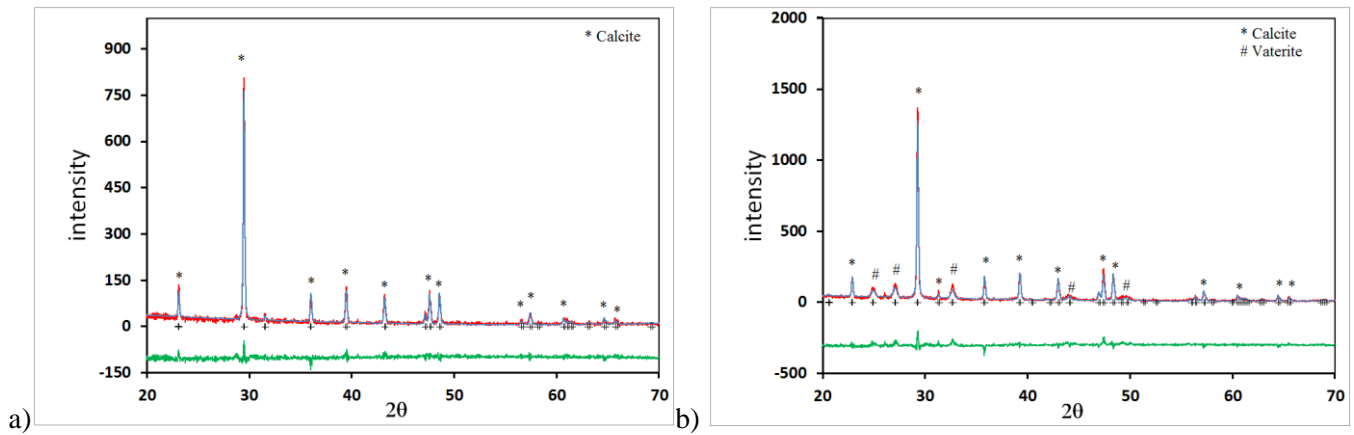
296 **Figure 5.** XRD patterns of NAN (a), CAL (b) and LAQ (c) samples exposed to air in outdoor conditions for 1 hour (60-
 297 80%RH). Red line corresponds to Intensity observed, blue line to Intensity calculated and green line to the Intensity observed -
 298 Intensity calculated difference curve. The crystal phases are shown in brackets and the "+" symbol corresponds to the main
 299 peaks.

300

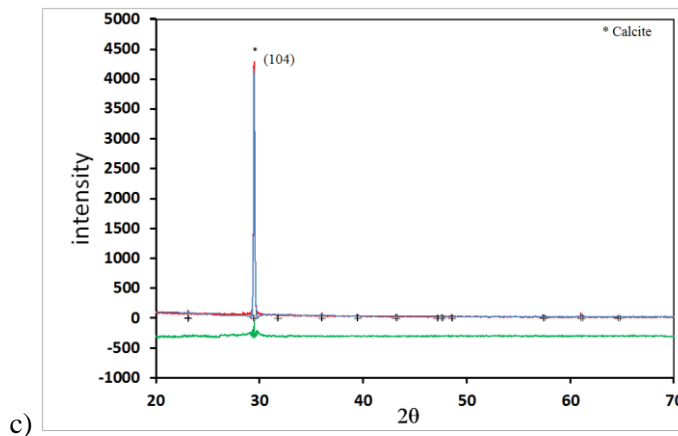
301 XRD analysis after 7 days of air exposure shows a better defined crystalline structure for all three samples (Fig. 6)
 302 resulting from the completion of the carbonation process. Both NAN and LAQ samples consist entirely of calcite
 303 (CaCO_3 , ICSD# 01-086-2334 and ICSD #01-083-0578 respectively) while CAL is composed of 75.8% of calcite
 304 (CaCO_3 , ICSD# 01-081-2027) and 24.2% of vaterite (ICSD# 01-072-0506). Vaterite is the least stable polymorph
 305 of calcium carbonate, calcite being the most stable one [29, 30]. In previous studies [24], Calosil was found to
 306 precipitate as calcite and aragonite. XRD-Rietveld shows the calcite crystals in LAQ (Fig. 6c) are fully oriented to
 307 {104} while the crystals in NAN and CAL have no preferred orientation. The Rietveld refinement factors are
 308 included in Table 1.

309

310



311



312

Figure 6. XRD patterns of NAN (a), CAL (b) and LAQ (c) samples exposed to air in outdoor conditions for 7 days (60-80%RH). Red line corresponds to Intensity observed, blue line to Intensity calculated and green line to the Intensity observed - Intensity calculated difference curve. The crystal phases are shown in brackets and the "+" symbol corresponds to the main peaks.

316

317

318

319

320

321

322

323

324

325

TEM images taken after 1 minute of air exposure show that during the carbonation process NAN and CAL tend to grow mainly as hexagonal plates (Fig. 7a, b) while LAQ nanoparticles can be seen to grow preferentially through the {010} side plane (Fig. 7c). SEM images taken after 7 days exposure to outdoor conditions show NAN and CAL being characterised by calcium carbonate crystals of irregular shape (Fig. 7d - 7e), while LAQ shows calcite in well-formed hexagonal prisms and parallelepiped shapes (Fig. 7f), presenting larger size (10 μ m) than NAN and CAL ones, despite the smaller original nanoparticle size. Prismatic calcite crystals with similar shape to that observed for LAQ have been described by Ukrainczyk *et al* [49] when examining the influence of additives on the growth of calcite crystals.

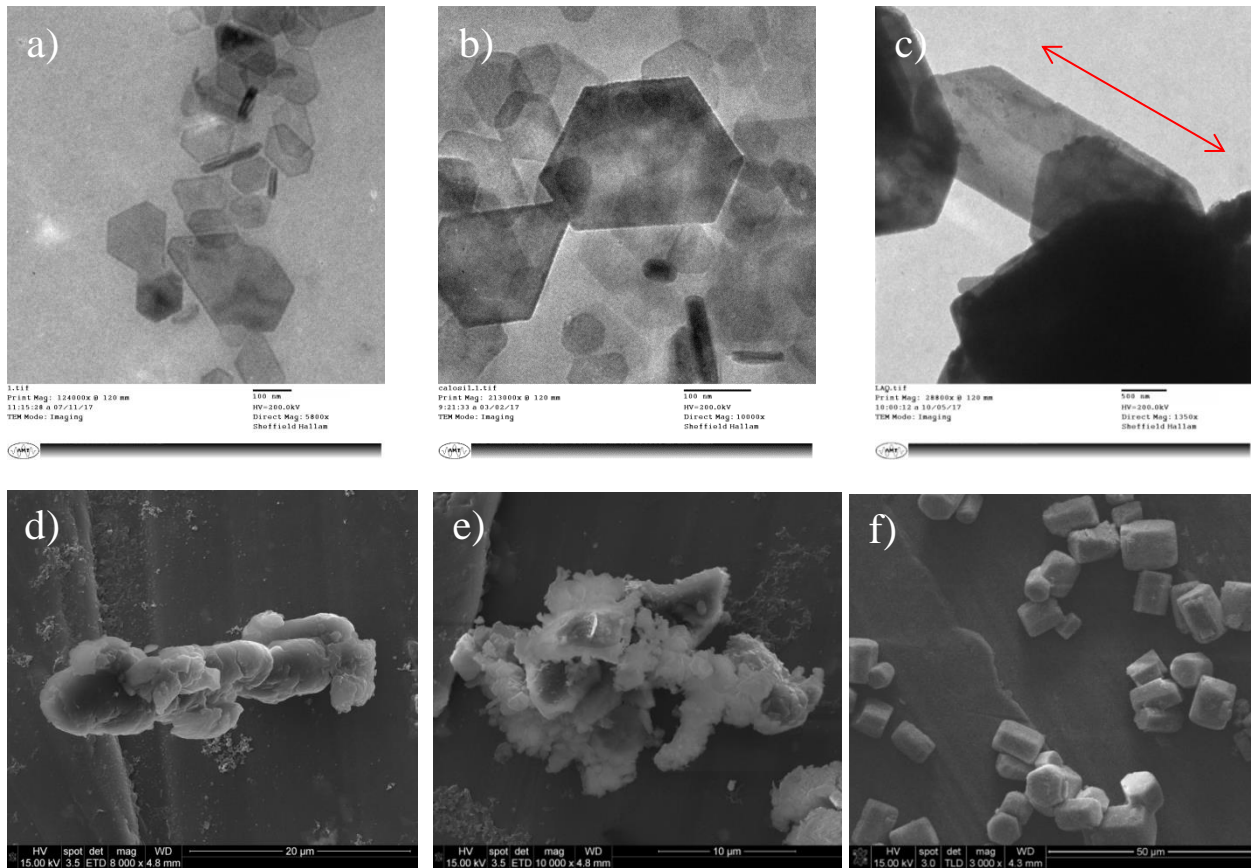


Figure 7. a) TEM image of NAN after 1 minute of air exposure at 124,000x; b) TEM image of CAL after 1 minute of air exposure at 213,000x; c) TEM image of LAQ after 1 minute of air exposure at 28,800x; d) SEM image of NAN after 7 days at 8,000x; e) SEM image of CAL after 7 days at 10,000 x; f) SEM image of LAQ after 7 days at 3,000x.

3.3 Effectiveness of the nanolime treatments

The pore structure properties of treated and control mortars are summarised in Table 2. It is evident that all three treatments affect the pore structure of the mortar by reducing the modal pore diameter and the porosity while increasing the total pore surface area. The highest porosity decrease was observed for the mortar treated with NAN (26% decrease), followed by those treated with LAQ (21%) and CAL (16%). The pore size distributions of control and treated mortars are shown in Fig. 8. It can be seen that the control sample has a tri-modal pore size distribution, coarser pores with diameters between 25 μm and 100 μm , intermediate pores with diameters between 3 μm and 25 μm and finer pores with diameters between 0.06 μm and 0.7 μm . Following the treatments, a complete removal of the coarsest mode and enhancement of the intermediate mode can be observed (Fig 8). Such enhancement is more prominent for the mortar treated with CAL (Fig. 8), which is in line with the lower decrease in porosity observed for this mortar.

344

345

Table 2. Pore structure properties of treated and control mortar samples measured by MIP

Sample	Porosity (%)	Modal pore diameter (μm)	Total pore surface area (m ² /g)
Control	22.63	18.09	0.45
NAN	16.75	15.23	0.575
CAL	18.92	13.55	0.585
LAQ	17.87	14.15	0.781

346

347

348

Figure 8. Differential volume of intruded mercury versus pore diameter of treated and control mortar samples

349

350

The water absorption and drying curves are reported in Fig 9. Apparent porosity by immersion, water absorption

351

and drying characteristics are reported in Table 3.

352

353

Page 16 of 30

354 **Figure 9.** Capillary absorption (a) and drying curves (b) for control and NAN, CAL and LAQ treated mortars

355

Table 3. Apparent porosity by immersion, capillary water absorption and drying characteristics

Parameter	CO	NAN	CAL	LAQ
Apparent porosity (%)	11.84 (± 0.20)	10.49 (± 1.63)	11.60 (± 0.40)	11.17 (± 0.65)
Water absorption coefficient ($10^{-3} \text{g/cm}^2 \text{s}^{0.5}$)	9.5 (± 0.78)	5.5 (± 1.7)	8.2 (± 2.5)	9.1 (± 0.5)
Water absorbed at asymptotic value (g)	11.00 (± 0.06)	8.95 (± 1.05)	10.60 (± 0.52)	10.32 (± 0.68)
Water absorbed after 24-hour immersion (g)	11.57 (± 0.16)	10.34 (± 1.61)	11.49 (± 0.38)	11.07 (± 0.50)
Initial drying rate ($10^{-3} \text{g/cm}^3 \text{h}$)	4.9 (± 0.1)	3.9 (± 0.3)	4.4 (± 0.5)	4.4 (± 0.3)
Final drying rate ($10^{-3} \text{g/cm}^3 \text{h}$)	1.0 (± 0.3)	1.0 (± 1.0)	1.2 (± 0.6)	1.2 (± 0.5)
Moisture content after 72 hours (g/cm^3)	0.01 (± 0.01)	1.81 (± 0.01)	1.94 (± 0.02)	2.02 (± 0.02)
Time for total drying (h)	± 50	> 72	> 72	> 72

Values in parentheses are standard deviation of the three cubic samples.

356

357 Capillary rise in a porous material is strongly influenced by pore size distribution. The pore diameter range
 358 affecting water capillary rise and transport could theoretically be considered to range between 1 mm and 1 μm
 359 diameter [50]. It is shown that all three treatments yield a decrease of the capillary water absorption coefficient of
 360 the mortar. This decrease can be attributed to the reduction in the number of pores with diameters between 17 μm
 361 and 100 μm , which results from the applied treatments and was also recorded by the MIP measurements. Figure 9a
 362 and Table 3 show that the NAN treatment yielded the biggest decrease in WAC (42%), followed by CAL (14%)
 363 and LAQ (4%). Control samples required about 7 hours of contact with water to reach asymptotic values while
 364 treated samples took nearly 9 hours (Fig. 9a). The latter absorbed less water by both capillarity and 24-hour
 365 immersion, with the NAN treated sample showing the greatest decreases.

366

367 The treatments also reduced the apparent porosity of the mortar, with the NAN treated samples showing the highest
 368 reduction (11.4%) followed by LAQ (5.7%) and CAL (2.1%). These results are fully compatible with the results of
 369 the porosity measurements by MIP reported above. The average apparent porosity of the treated samples show a
 370 relatively high standard deviation reflecting the inhomogeneity of the applied treatment, with the CAL (± 0.40)
 371 being only twice the value of the control, while LAQ (± 0.65) is thrice higher than the control and NAN (± 1.63)
 372 being significantly higher (Table 3).

373

374 The drying curves (Fig. 9b) and the measured initial and final drying rates (Table 3) show that treated mortar
 375 samples take far more time to dry than the control ones. This is an undesirable behaviour as it increases the risk of
 376 spalling when the mortar is exposed to freeze-thaw cycles (limited to the external 1 cm plus where the nanolime
 377 precipitates) and / or biological attack [51]. The drying rate reduction is attributed to the finer pore structure of the
 378 mortar near the surface of the sample which results from the nanolime treatment. The smaller pores in the denser
 379 mortar layer reduce the liquid water transport towards the surface hence slowing down the drying kinetics [51]. The
 380 lowest initial drying rate was observed for the mortar treated with CAL while NAN and LAQ yielded similar rates.
 381 Whilst control samples were completely dry after 50 hours, treated samples still contained some residual moisture
 382 after 72h (Table 3).

383
 384 Table 4 shows the results of the Scotch Tape Test (STT). A significant decrease of removed material ($\Delta V \approx 90\%$)
 385 was observed for all treated mortars with no significant differences in the performance of the three nanolimes. The
 386 standard deviation of the ΔV (%) (SD) shown in the table confirms a good reliability for this test in the measuring
 387 of surface cohesion.

Table 4. Scotch tape test results. Values determined on 9 measurements.

Treatment	Removed material (mg/cm ²)		ΔV (%)	SD
	Before treatment	After treatment		
NAN	26.85 (± 1.24)	2.54 (± 3.96)	90.54	5.1
CAL	26.71 (± 1.56)	1.71 (± 0.73)	93.60	2.3
LAQ	26.76 (± 1.04)	3.16 (± 2.57)	88.19	3.6

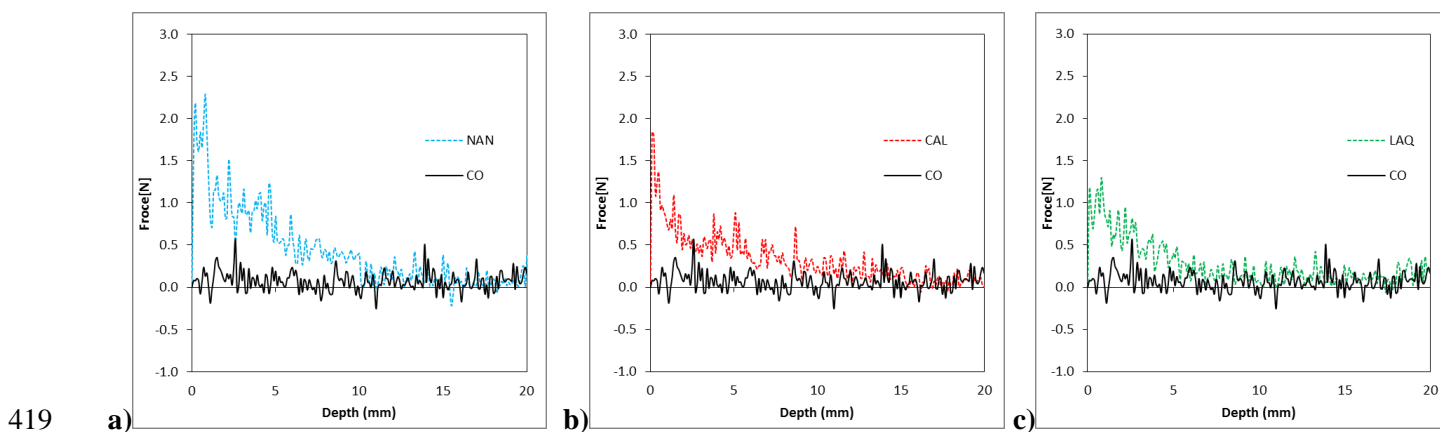
Scotch area: 3 x 1.5 cm; Values in parentheses are standard deviation for the nine measurements taken on each of the three cub samples

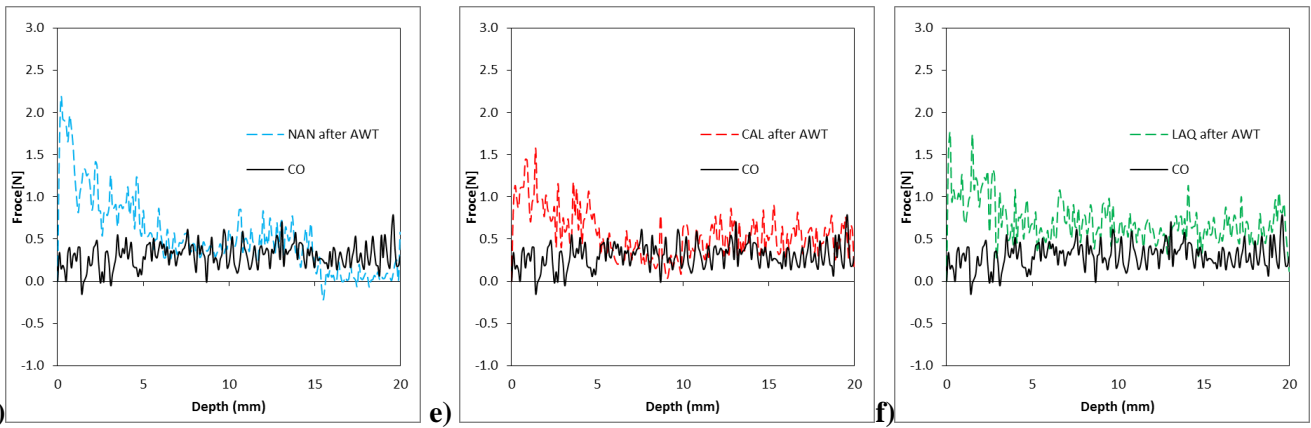
389
 390 Drilling resistance results are shown in Figure 10. It can be seen that whilst the control sample shows a steady
 391 drilling resistance throughout the drilling depth (average force $\approx 0.07N$), the treated samples show increased
 392 resistance within the first 10 mm from the surface. The highest average drilling resistance was observed for the
 393 mortar treated with NAN (average force ≈ 0.57), followed by those treated with CAL (average force ≈ 0.32) and
 394 LAQ (average force ≈ 0.27). This is fully compatible with the porosity results which showed a more marked
 395 decrease of porosity for NAN treated samples than for CAL and LAQ treated samples. The average drilling
 396 resistance in the outer 5 mm is 0.09 N for Control, 1.12 N for NAN, 0.68 N for CAL and 0.64 N for LAQ, which is
 397 also in line with the results of the MIP measurements. This trend was not observed in the results of the Scotch Tape

398 Test, possibly due to a lower sensitivity of this technique compared to that of the DRMS. The DRMS profiles in
399 Figure 10a-c show that the drilling resistance of the treated samples decreases with depth until it reaches the
400 resistance of the control sample at about 10 mm for NAN and CAL and about 6 mm for LAQ. This data seems to
401 indicate for the NAN and CAL treatments a deeper penetration into the mortar compared to the LAQ treatment.
402

403 The drilling resistance tests were repeated after exposing the samples to alternating cycles of UV light and moisture
404 (Fig. 10d-f) and the results show for the NAN and CAL treated samples a reduction of the depth at which the
405 drilling resistance reaches that of the control samples. This could indicate that a certain amount of material got
406 partially dissolved from the surface of these samples as a result of the exposure to the alternating cycles of UV light
407 and moisture condensation at elevated temperatures in the tester. The presence of deposits of white powder material
408 in the water pan just below the sample holder panel seems to support this interpretation. The DRMS profile of the
409 LAQ treated sample is similar to that recorded before the accelerated weathering test (Fig. 10f), which seems to
410 indicate that less or no material loss occurred on the surface of this sample. The apparent higher resistance to
411 weathering of the LAQ treated sample compared to that of the NAN and CAL treated ones could be attributed to a
412 better developed crystalline structure and larger crystals. As described in section 3.2, LAQ produces perfectly
413 shaped prismatic and parallelepiped calcite crystals of a larger size compared to NAN and CAL, which present
414 poorly crystallized ones. The "well-shaped" calcite crystals are more resistant to dissolution than irregular shaped
415 crystals as is well known [52]. In the case of the CAL treated sample, a reduction of the drilling resistance was
416 observed within the first millimeter of depth (Fig. 10e), which could be due to the solubility of metastable
417 amorphous carbonate phases such as vaterite (see section 3.2).

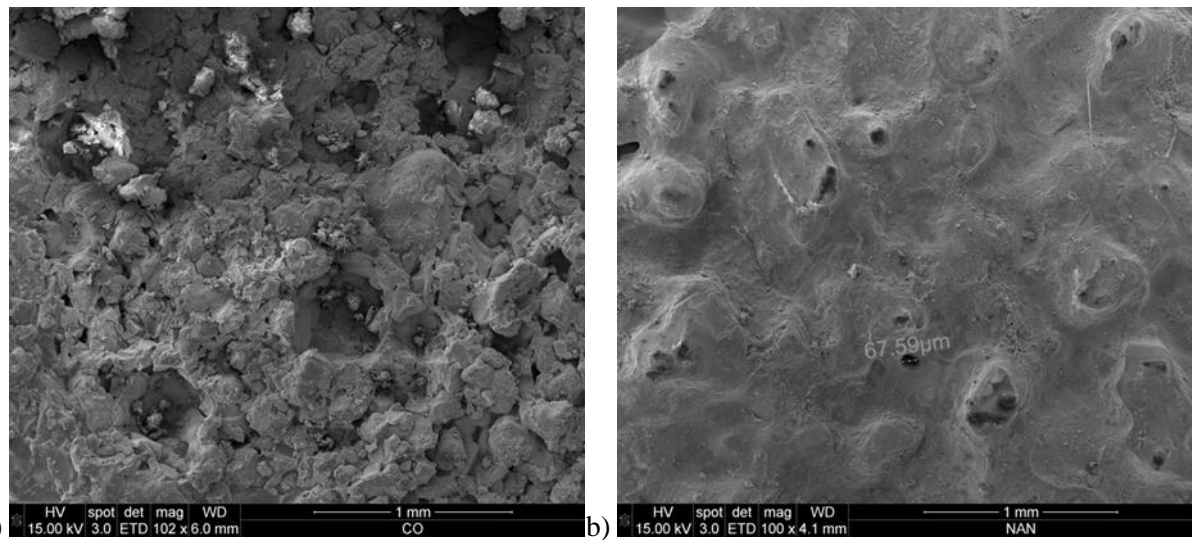
418



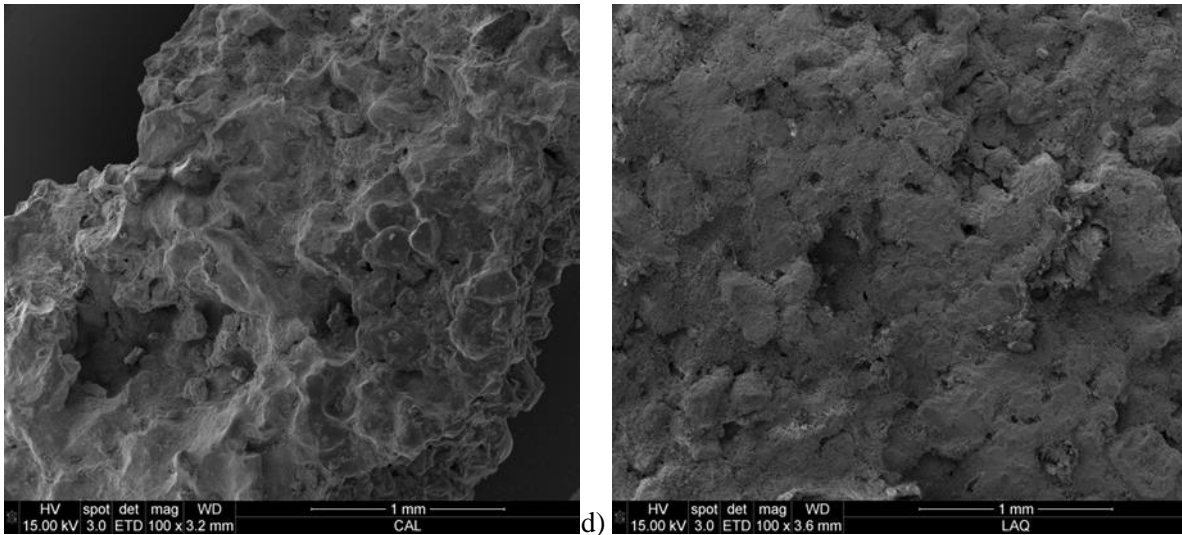


420 **d)** **e)** **f)**
 421 **Figure 10.** Drilling resistance of: a) NAN; b) CAL; c) LAQ; d) NAN after AWT; e) CAL after AWT and f) LAQ after AWT.
 422

423 Both treated and untreated mortar surfaces were observed by SEM in order to study the distribution of the nanolime
 424 in the pores and the morphology of the calcite crystals. SEM micrographs showed for the control samples a great
 425 number of large pores (pore diameter >100 μm), which are outside of the measurement range of the used MIP
 426 technique (Fig.11a). Following the treatments, the reduction of porosity and pore size due to the deposition of
 427 calcite inside the pores is clearly visible (Fig. 11b-d).



428 a) b)



429

c) d)

430

Figure 11. SEM micrographs of mortar samples (100 X): a) control sample; b) surface treated with NAN; c) surface treated with CAL; d) surface treated with LAQ.

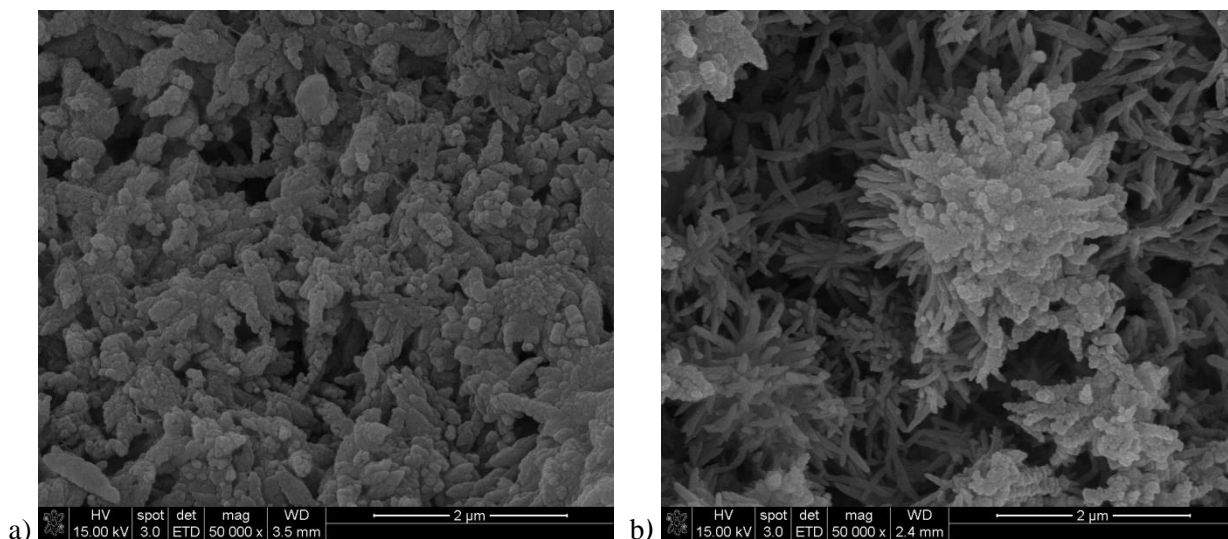
432

433

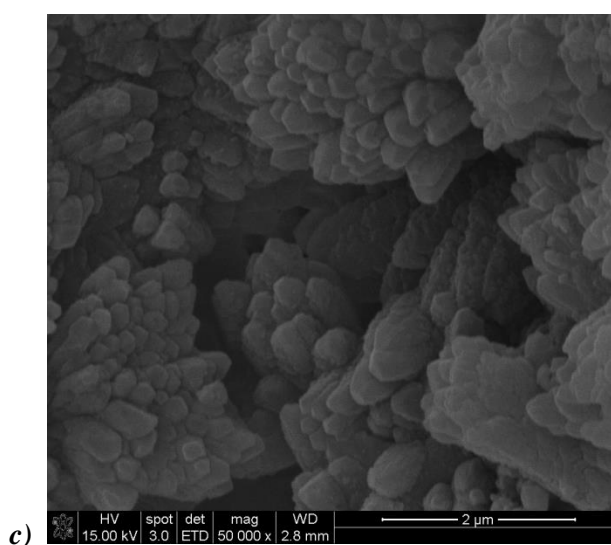
In Figures 11 b-d it can be seen that the nanolime is distributed homogeneously in the pores of the mortar and seems to adhere well to the substrate to the point that it is not easy to distinguish between the mortar and the newly precipitated calcite which fills the pores reducing their size. Fig. 12a shows that the calcitic material resulting from the carbonation of NAN within the mortar presents a different variety of shapes (mostly rhombohedral with scalenohedral terminations), which were observed also in previous studies for the same nanolime [24]. CAL precipitated in the form of calcite rhombohedra and some vaterite (Fig. 12b). Fig 12c shows typical calcite prisms on the LAQ sample. These are larger than those formed by NAN and CAL hence resulting in a smaller specific surface which is associated with higher resistance to weathering [52]. This morphology is similar to that visible on the SEM images (section 3.2).

442

443



444



445

Figure 12. SEM detail micrographs of carbonated nanolime : a) NAN 50,000x; b) CAL 50,000x; c) LAQ 50,000x.

446

447

Ideally consolidation treatments should improve the physical-mechanical properties of the treated material without

448

affecting its aesthetic appearance. However, a common side effect of the use of nanolime is a whitening of the

449

surface following treatment. In order to investigate the occurrence of this phenomenon in association with the use

450

of the tested nanolimes, spectrophotometric analyses were carried out to measure changes in L^* (white-black

451

parameter) and ΔE^* (total colour variations) following treatment. ΔE^* values < 5 are considered suitable for

452

practical conservation interventions and visually imperceptible [28]. The results (Table 5) show that all of the three

453

treatments cause whitening of the surface with both ΔE^* and ΔL^* values above 5. NAN yielded the lowest

454

whitening effect ($\Delta L^* \approx 6$ and total colour alteration $\Delta E^* \approx 6$). CAL and LAQ caused a more significant

455

whitening effect with $\Delta L^* \approx 7.5$ and $\Delta L^* \approx 11.94$, respectively, and total colour change with $\Delta E^* \approx 9$ and $\Delta E^* \approx 14$,

456 respectively. In previous studies, NAN and CAL yielded chromatic alterations of about $\Delta E^* \approx 6$ and $\Delta E^* \approx 4$,
 457 respectively [24]. The lower colloidal stability of LAQ is considered responsible for the more significant formation
 458 of undesired surface whitening. Nonetheless, the observed whitening and total chromatic alterations are still lower
 459 than those caused by the lime-water technique, which normally vary between $\Delta L^* \approx 50$ to 70 [9, 25].

460

461 The whitening effect and total colour changes associated with the application of nanolime decreased after the
 462 samples were exposed to UV light and moisture cycles in the accelerated weathering test, with both ΔE^* and ΔL^*
 463 decreasing below 5. This could indicate that the induced weathering dissolved a certain amount of material from
 464 the surface of the samples, as also detected by the DRMS for the NAN and CAL samples. It is apparent that in the
 465 case of the LAQ samples the amount of material that got dissolved from their surface during the accelerated
 466 weathering test was sufficient to reduce the whitening but too small to be detected by the DRMS.

467

468

Table 5. Chromatic alterations of treated samples before and after the Accelerated Weathering Test.

	ΔL^*		Δa^*		Δb^*		ΔE^*	
	Treated	AWT	Treated	AWT	Treated	AWT	Treated	AWT
NAN	6.33 (± 0.20)	3.18 (± 0.43)	-1.48 (± 0.16)	-0.48 (± 0.20)	-0.43 (± 0.91)	-1.96 (± 0.55)	6.51	3.76
CAL	7.50 (± 0.51)	2.53 (± 0.90)	-0.75 (± 0.13)	-0.37 (± 0.16)	-4.64 (± 0.69)	-0.88 (± 1.15)	8.85	2.7
LAQ	11.94 (± 0.96)	4.04 (± 0.63)	-1.25 (± 0.15)	-0.55 ($\pm 0.0.26$)	-6.96 (± 1.07)	-1.17 (± 1.45)	13.87	4.24

Values determined on 30 measurements; AWT (Accelerated Weathering Test)

469

470

471 Conclusions

472 This study has shown that NAN, CAL and LAQ can be used effectively for the consolidation of highly porous
 473 calcareous materials such as lime mortars and represent a viable alternative to organic consolidants for their
 474 consolidation. It has been proven that repeated applications of low concentration dispersions of these nanolimes can
 475 restore the substrate superficial cohesion, improve its mechanical properties, reduce its porosity, number of
 476 micropores (10 - 100 μm) and water absorption coefficient.

477

478 It has been shown that:

- 479 • The $\text{Ca}(\text{OH})_2$ nanoparticles of the three nanolimes consist of crystalline hexagonal plates with similar
480 shapes. However, there is a difference in size: LAQ nanoparticles are smaller than both NAN and CAL.
481 XRD-Rietveld refinements showed that LAQ $\text{Ca}(\text{OH})_2$ particles tend to align in a preferential direction
482 along the side plane $\{010\}$ whereas NAN and CAL did not show any significant preferred orientation.
483 Nanorestore Plus® and Calosil® are stable colloidal dispersions while LAQ nanoparticles start to settle
484 about 2 min after agitation (sedimentation rate $\approx 6\%$ per h) and the 12% of the particles has settled after 2
485 hours. This sedimentation rate is considered acceptable for practical purposes as most of the particles
486 remain in colloidal state during the time of the application. However, a moderate agitation is highly
487 recommended before the application of this nanolime. Moreover, the application should ideally be
488 completed within the first 2 first minutes after the agitation, before the particles start to settle.
- 489 • Nanolime particles created by anion exchange synthesis (LAQ) are the most reactive with calcite being the
490 only detected crystalline phase after 1 hour of air exposure. NAN particles also showed a good reactivity
491 with 90% of the sample being composed of calcite following the same exposure time. CAL particles
492 showed slower carbonation and no calcite had formed after 1 hour exposure. After 7 days both LAQ and
493 NAN consisted entirely of calcite, while CAL was composed approximately of 75% of calcite and 25% of
494 vaterite, which is a metastable phase of calcium carbonate, less stable than calcite.
- 495 • During the carbonation process, NAN and CAL tend to grow mainly as hexagonal plates while LAQ
496 nanoparticles seem to grow preferentially through the $\{010\}$ side plane. After 7 days of carbonation, LAQ
497 shows well-formed hexagonal calcite prismatic crystals with larger size than NAN and CAL, which
498 consist of calcite crystals of irregular shape. XRD-Rietveld shows the calcite crystals in LAQ are fully
499 oriented to $\{104\}$ while the crystals in NAN and CAL have no preferred orientation.
- 500 • All treatments affect the pore structure by reducing the porosity of the superficial portion of the mortar.
501 The reduction in porosity is attributed mainly to a reduction of the number of pores with diameter between
502 $17\mu\text{m}$ and $100\mu\text{m}$, which also decreases the capillary water absorption coefficient. Nanorestore Plus®
503 presented the highest reduction of the porosity and water absorption by capillarity rate.
- 504 • All three nanolimes increase the drilling resistance of the mortar surface. The penetration depth of
505 nanolime appears to be approximately 1 cm for NAN and CAL and 0.6 cm for LAQ. NAN treated mortars
506 showed the highest increase in drilling resistance, which is in line with their highest reduction in porosity;

507 followed by those treated with CAL and LAQ. Following an accelerated weathering test, the DRMS
508 detected the loss of a certain amount of material from the surface of mortars treated with NAN and CAL.
509 This was not observed for LAQ treated samples, possibly due to LAQ better developed crystalline
510 structure providing higher resistance to dissolution processes during the accelerated weathering test. The
511 detected loss is slightly more pronounced in Calosil® samples, possibly as a consequence of the
512 dissolution of metastable vaterite. A study of the calcite morphology and structural features of LAQ
513 nanolime must be addressed in future studies to better understand the performance of this nanolime.

- 514 • Following treatment, the samples take far more time to dry due to a finer pore structure of the mortar near
515 the surface. This is an undesirable behaviour which may lead to deterioration processes. Specifically,
516 spalling can occur where moisture is present and the mortar is exposed to freeze-thaw cycles. Furthermore,
517 longer drying times can favour biological growth and the dissolution of poorly crystallised calcite and
518 vaterite. A full study of the durability of mortars treated with the three nanolimes will be carried out in
519 future research.
- 520 • All treatments produced an undesired whitening of the surface after application. LAQ treatment induced
521 the highest whitening effect which can be attributed to the lower colloidal stability of this nanolime. The
522 whitening effect associated with all treatments decreases to values which are imperceptible to the naked
523 eye after exposing the samples to the Accelerated Weathering Test. This could indicate that a superficial
524 layer of the consolidated mortar was partially dissolved during the accelerated weathering test, as also
525 observed by DRMS. In the case of LAQ treated mortars the dissolution decreased the whitening without
526 causing significant thickness reduction.

527
528 One final conclusion of this study is that substrates treated with the studied nanolimes will require regular
529 maintenance (i.e. periodic application of nanolime) in order to achieve long term performance in terms of
530 mechanical and physical properties. Further work carried out by the authors has focused on the influence of the use
531 of different types of solvents on the performance of LAQ nanolime and a report will be submitted for publication in
532 due course.

533
534 **Declaration of conflicting interests**

535 The authors declare that there is no conflict of interest and take a neutral position to offer an objective evaluation of
536 the consolidation process.

537

538 **Acknowledgements**

539 This research has been funded by a Vice Chancellor's Scholarship within the Doctorate Program at Sheffield
540 Hallam University (UK). The authors want to thank Dr. Anthony Bell for his support with Rietveld refinements.

541

542 **References**

543 [1] Doehne E., Price C. A., (2011), *Stone Conservation: An Overview of current research, 2nd edition*, Research in
544 Conservation, The Getty Conservation Institute, Getty Publications, Los Angeles, pp. 35-37.

545 [2] Charola A. E., Ware. R., (2002), Acid deposition and the deterioration of stone: a brief review of a broad topic.
546 Siegesmund GS, Vollbrecht A, Weiss T., (eds) *Natural stone, weathering phenomena, conservation strategies and*
547 *case studies*, Special Pu (London), pp. 393–406. Available at: doi:10.1144/GSL.SP.2002.205.01.28 .

548 [3] Hansen E., Doehne E., Fidler J., et. al. (2013), A review of selected inorganic consolidants and protective
549 treatments for porous calcareous materials”, *Reviews in Conservation*, vol. 4, pp. 3630.

550 [4] Young, M. E., Murray M., and Cordiner P., (1999), *Stone consolidants and chemical treatments in Scotland*.
551 Report to Historic Scotland.

552 [5] Ambrosi, M., Dei L., Giorgi R., et. al., (2001), Colloidal particles of Ca(OH)₂: properties and applications to
553 restoration of frescoes, *Langmuir*, vol. 17 (14), pp. 4251–4255. Available at:
554 <http://pubs.acs.org/doi/abs/10.1021/la010269b>.

555 [6] Henriques, F., Charola, A. E., (1996), A comparative study of standard test procedures for mortars, *Proceedings*
556 *of the 8th International Congress on Deterioration and Conservation of Stone*, pp. 1521-1528.

557 [7] Price, C., Ross, K., White, G., (1988), A further appraisal of the 'Lime Technique' for limestone consolidation ,
558 using a radioactive tracer. *IIC journal.Studies in Conservation*, vol. 33 (4), pp.178–186.

559 [8] Brajer I., Kalsbeek N., (1999), Limewater absorption and calcite crystal formation on a limewater-impregnated
560 secco wall-painting, *Studies in Conservation* vol. 44 (3), pp. 145–156.

561 [9] Slizkova, Z., Dracky M., Viani A., (2015), Consolidation of weak mortars by means of saturated solution of
562 calcium hydroxide or barium hydroxide, *Journal of Cultural Heritage*, vol. 16, No. 4, pp. 420-460..

- 563 [10] Bracci, S., Sacchi, B., Pinto, A. F., et. al., (2008), Inorganic consolidants on stone artifacts: optimization of
564 application procedures for marble and limestones". International Symposium "Stone consolidation in cultural
565 heritage: research and practice", Lisbon 6-7 May, 2008. Proceedings, J. Delgado Rodrigues & João Manuel
566 Mimoso (Eds.), pp. 81-90.
- 567 [11] Wheeler, G., (2005), Alkoxysilanes and consolidation of stone, The Getty Conservation Institute, Getty
568 Publications, Research in Conservation, Los Angeles., pp. 31 - 48.
- 569 [12] Charola A. E., Tucci A., (1986), On the reversibility of treatments with acrylic/silicone resin mixtures. Journal
570 of the American Institute for Conservation, Vol. 25, pp. 83–92.
- 571 [13] Charola A. E., (1995), Water-repellent treatments for building stones : A practical Overview. Association for
572 Preservation Technology International (APT), vol. 26 (2), pp.10–17. Available at:
573 <http://www.jstor.org/stable/1504480>.
- 574 [14] Jroundi F., Fernández-Vivas A., Rodríguez-Navarro C., et. al., (2010), Bioconservation of deteriorated
575 monumental calcarenite stone and identification of bacteria with carbonatogenic activity, Microbial Ecology vol.
576 60, pp. 39–54.
- 577 [15] Baglioni P., Carrasco-Vargas R., Chelazzi D., et. al., (2006), The maya site of Calakmul: In situ preservation
578 of wall painting and limestone using nanotechnology, Studies in Conservation, 51:2, 162-169, DOI:
579 10.1179/sic.2006.51.Supplement-2.162
- 580 [16] Otero J., Charola A. E., Grissom C., et al., (2017), "An overview of nanolime as a consolidation method for
581 calcareous substrates". Ge-Conservación Journal, vol. 11 (1), pp. 71-78. DOI:10.17265/2162-5298.
- 582 [17] Taglieri G., Daniele V., Macera L., et al., (2017), Nano Ca(OH)₂ synthesis using a cost-effective and
583 innovative method: Reactivity study, J.Am Ceram Soc. 2017;100:5766–5778.
- 584 [18] Taglieri G., Felice B., Daniele V., et al., (2016), Analysis of the carbonatation process of nanosized Ca(OH)₂
585 particles synthesized by exchange ion process, Proceedings of the Institution of Mechanical Engineers, Part N:
586 Journal of Nanoengineering and Nanosystems vol. 230 (1), pp. 25-31.
- 587 [19] Volpe R., Taglieri G., Daniele V., et. al., (2016), A process for the synthesis of Ca(OH)₂ nanoparticles by
588 means of ionic exchange resin, European patent EP2880101.
- 589 [20] Baglioni P., Chelazzi D., Giorgi R., et. al., (2014), Commercial Ca(OH)₂ nanoparticles for the consolidation of
590 immovable works of art, Applied Physics A vol. 114, pp. 723–732.

- 591 [21] Costa D., Delgado Rodrigues J., (2012), Consolidation of a porous limestone with nanolime, in: Proceeding of
592 12th International Congress on Deterioration and Conservation of Stone, Columbia University, New York, October
593 22–26.
- 594 [22] Campbell A., Hamilton A., Stratford T., et. al., (2011), Calcium hydroxide nanoparticles for limestone
595 conservation: imbibition and adhesion, Proceedings of Symposium Adhesive and Consolidants for Conservation:
596 Research and Applications, ICC, Ottawa, October 17–21.
- 597 [23] Ghaffari E., Koberle T., Weber J., (2012), Methods of polarising microscopy and SEM to assess the
598 performance of nanolime consolidants in porous solids, Proceeding of 12th International Congress on Deterioration
599 and Conservation of Stone, Columbia University, New York, October 22–26.
- 600 [24] Arizzi A., Gomez-Villalba L. S., Lopez-Arce P., et. al., (2013), Lime mortar consolidation with nanostructured
601 calcium hydroxide dispersions: the efficacy of different consolidating products for heritage conservation, European
602 Journal of Mineralogy, vol. 27 (3), pp. 311–323.
- 603 [25] Slizkova Z., Frankeová D., (2012), Consolidation of a porous limestone with nanolime, Proceedings of the
604 12th International Congress on the Deterioration and Conservation of Stone, New York.
- 605 [26] Borsoi G., Lubelli B., Van Hees R., et. al., (2016), Understanding the transport of nanolime consolidants
606 within Maastricht limestone, Journal of Cultural Heritage vol. 18, pp. 242-24.
- 607 [27] Ruffolo S. A., La Russa M. F., Aloise P., et. al., (2014), Efficacy of nanolime in restoration procedures of salt
608 weathered limestone rock, Applied Physics A Materials Science & Processing vol. 114, pp. 753-758.
- 609 [28] Rodriguez-Navarro C., Suzuki A., Ruiz-Agudo E., (2013), Alcohol dispersions of calcium hydroxide
610 nanoparticles for stone conservation, Langmuir vol. 29, pp. 11457–11470.
- 611 [29] López-Arce, P., Gomez-Villalba, L. S., Pinho, L., et. al., (2010), Influence of porosity and relative humidity on
612 consolidation of dolostone with calcium hydroxide nanoparticles: effectiveness assessment with non-destructive
613 techniques, Materials Characterization Journal, vol. 61, pp. 168-184.
614 <http://dx.doi.org/10.1016/j.matchar.2009.11.007>.
- 615 [30] Lopez-Arce, P., Gomez-Villalba, L. S., Martinez-Ramirez, et. al., (2011), Influence of relative humidity on
616 the carbonation of calcium hydroxide nanoparticles and the formation of calcium carbonate polymorphs. Powder
617 Technology, vol. 205, pp. 263-269. <http://dx.doi.org/10.1016/j.powtec.2010.09.026>.
- 618 [31] Rodriguez-Navarro C., Vettori I., Ruiz-Agudo E., (2016), Kinetics and mechanism of calcium hydroxide
619 conversion into calcium alkoxides: Implications in heritage conservation using nanolimes, Lagmuir, DOI:
Page 28 of 30

620 10.1021/acs.langmuir.6b01065.

621 [32] Taglieri G., Otero J., Daniele V., et. al., (2017), The biocalcarene stone of Agrigento (Italy): Preliminary
622 investigations of compatible nanolime treatments, Journal of Cultural Heritage,
623 <https://doi.org/10.1016/j.culher.2017.11.003>.

624 [33] The European Standard EN 1015-3:1990, (1990), Methods of test for mortar for masonry. Determination of
625 consistence of fresh mortar (by flow table).

626 [34] The European Standard EN 1015-2:1998, (1998), Methods of test for mortar for masonry. Bulk sampling of
627 mortars and preparation of test mortars.

628 [35] Rietveld H.M., A profile refinement method for nuclear and magnetic structures. Journal Applied
629 Crystallography, 10, 65, 1969.

630 [36] Bish D. L., Post J. E., (1989), Modern powder diffraction. Mineralogical Society of America, Washington.

631 [37] The English Standard EN 13755 for Natural stone test methods (2008). Determination of water absorption at
632 atmospheric pressure.

633 [38] ASTM C97-96 Standard Test Methods for Absorption and Bulk Specific Gravity of Dimension Stone, (2000),
634 ASTM International, West Conshohocken, PA, <https://doi.org/10.1520/C0097-96E01>.

635 [39] The European Standard CEN - EN 16322 (2013), Conservation of Cultural Heritage - Test methods -
636 determination of drying properties.

637 [40] ASTM D3359-02: Standard Test Methods for Measuring Adhesion by Tape Test, (2002), ASTM International,
638 10 August.

639 [41] Tiano P., Delgado Rodrigues J., De Witte E., et. al., (2000), The conservation of monuments: a new method to
640 evaluate consolidating treatments, International Journal for Restoration of Buildings and Monuments vol. 6 (2),
641 pp. 133-150.

642 [42] Pinto A. P., Delgado-Rodrigues J., (2008), Stone consolidation: the role of treatment procedures, Journal of
643 Cultural Heritage, vol. 9, pp. 38-53.

644 [43] Grossi, C. M., Blimblecombe, P., Esbert, R. M., et. al., (2007) Color changes in architectural limestones from
645 pollution and cleaning. Color Res. Appl. vol. 32, pp. 320–331.

646 [44] ASTM 6154 -4. Standard Test Method for the Accelerated Weathering test Method for QUV QUV/BASIC
647 Weathering Tester.

- 648 [45] Taglieri, G., Felice, B., Daniele, V., et. al, (2014), Analysis of the carbonation process of nanosized $\text{Ca}(\text{OH})_2$
649 particles synthesized by exchange ion process, Proceedings of the Institution of Mechanical Engineers, Part N:
650 Journal of Nanoengineering and Nanosystems DOI: 10.1177/1740349914537616.
- 651 [46] Ziegenbald, G., (2008), Colloidal calcium hydroxide – a new material for consolidation and conservation of
652 carbonate stone. Proceedings of 11th International congress on deterioration and conservation of stone III,
653 Lukaszewicz E&Niemcewicz P., eds., Torun, pp. 1109–1115.
- 654 [47] Borsoi, G., Lubelli, B., van Hees, R., et. al., (2015). Deposition of modified nanolimes within calcareous
655 substrates. 1-2. Abstract from Green Conservation of Cultural Heritage, 27-28 October 2015, Rome, Italy.
- 656 [48] Giorgi R., Dei L., Baglioni P., (2000), A new method for consolidating wall paintings based on dispersions of
657 lime in alcohol, Studies in conservation, vol. 45, vol. 3, pp. 154 - 161.
- 658 [49] Ukrainczyk, M., Greiner M., Elts E., et. al., (2015), Simulating preferential sorption of tartrate on prismatic
659 calcite surfaces, CrystEngComm Journal, vol. 17, 149-159. DOI: 10.1039/c4ce01447b.
- 660 [50] Charola A. E., Wendler E., (2015), An overview of the water-Porous building materials interactions,
661 Restoration of building and monuments Journal, vol. 21(2-3), pp. 55-63.
- 662 [51] Charola A. E., Vicenzi E. P., Grissom C. A., et. al., (2017), Composition and characteristics of Kasorta
663 limestones on the exterior of the National Museum of the American Indian Building. pp.17-26. J.Sledge, A. E.
664 Charola, P. T. DePriest and R. Koestler, eds. Conservation of the Exterior of the National Museum of the American
665 Indian Building, Smithsonian Contributions to Museum Conservation, N°. 6. ISSN 1949-2359.
- 666 [52] Charola, A. E., (1988), Chemical-physical factors in stone deterioration. Durability of Building Materials vol.
667 5, pp. 309-316.
- 668
- 669
- 670